Surrogate modelling of railway pantograph-catenary interaction using deep Long-Short-Term-Memory neural networks

Song, Yang; Wang, Hongrui; Frøseth, Gunnstein; Nåvik, Petter; Liu, Zhigang; Rønnquist, Anders

DOI
10.1016/j.mechmachtheory.2023.105386

Publication date
2023

Document Version
Final published version

Published in
Mechanism and Machine Theory

Mechanism and Machine Theory 187 (2023) 105386

Contents lists available at ScienceDirect

Mechanism and Machine Theory

journal homepage: www.elsevier.com/locate/mechmt

Research paper

Surrogate modelling of railway pantograph-catenary interaction using deep Long-Short-Term-Memory neural networks

Yang Song [a,b,c], Hongrui Wang [d,*], Gunnstein Frøseth [c], Petter Nåvik [c], Zhigang Liu [a], Anders Rønnquist [c]

[a] National Rail Transit Electrification and Automation Engineering Technique Research Centre, Southwest Jiaotong University, 611756, China
[b] SWJTU-Leeds Joint School, Southwest Jiaotong University, 611756, China
[c] Department of Structural Engineering, Norwegian University of Science and Technology, Trondheim 7491, Norway
[d] Department of Engineering Structures, Delft University of Technology, Deft 2628CN, The Netherlands

ARTICLE INFO

Keywords:
High-speed railway
Pantograph-catenary interaction
Deep learning
LSTM
Contact force
Surrogate model

ABSTRACT

The interaction performance of the pantograph-catenary is of great importance as it directly determines the current collection quality and operational safety of trains. The finite element method (FEM) is dominantly used for simulating pantograph-catenary interaction, which is normally computationally heavy. In this work, addressing the tremendous computational cost of FEM models, a surrogate model for fast simulations of pantograph-catenary interaction is proposed using deep learning. A dataset containing 30,000 cases of pantograph-catenary interaction is generated by a validated FEM model. A Long-Short-Term-Memory (LSTM) neural network is proposed to learn the inherent nonlinearity between the input model parameters and the output pantograph-catenary contact force from data. The resulting prediction performance indicates that contact forces predicted by the surrogate model are consistent with those simulated by FEM, while the computational efforts of the surrogate model are negligible compared with FEM. Prediction performances using different network architectures and configurations are compared to determine the optimal setting for a pantograph-catenary system. The LSTM-based surrogate model shows high efficiency for simulating pantograph-catenary interactions and promising practicability in optimising catenary structural parameters for design or upgrade.

1. Introduction

In electric railways, the pantograph-catenary system, as schematically shown in Fig. 1, is widely used to transmit continuous electric energy to locomotives. The mechanical interaction between the pantograph and catenary is of great importance, as a stable sliding contact is the prerequisite of a good current collection quality. With the global booming of high-speed railways, the study of pantograph-catenary interaction has attracted ever-increasing attention from both academia and industry [1].

1.1. Problem description

Numerical simulation is the most widely-adopted approach to reproduce the realistic behaviour of pantograph-catenary interaction

* Corresponding author.
E-mail address: H.Wang-8@tudelft.nl (H. Wang).

https://doi.org/10.1016/j.mechmachtheory.2023.105386
Received 20 October 2022; Received in revised form 27 April 2023; Accepted 28 April 2023
Available online 3 May 2023

without huge economic cost [2]. These simulations, often based on the finite element method (FEM), are generally computationally heavy. However, the emerging concept of digital twins requires simulations of physical systems to be accurate, efficient, and interactable with real-world data. To alleviate the computational burden of complex mathematical models, the approximation or surrogate modelling of physical models has been state-of-the-art in rail engineering, as demonstrated in Refs. [3–5]. It provides the opportunity to discover the optimal design and upgrade of physical systems economically and timely. The recent and rapid development of artificial intelligence (AI) makes it feasible to approximate physical models with high accuracy *via* surrogate modelling [6]. Unlike a fast-integration algorithm, a data-based model has very little computational cost once trained. This paper attempts to investigate the possibility of learning a surrogate model from a finite element (FE) model of pantograph-catenary interaction using deep learning.

1.2. Literature review

Nowadays, various types of pantograph-catenary numerical models have been developed worldwide. In 2016, Bruni et al. [7] compared the results of some mainstream ones to set up a benchmark for the validation of numerical accuracy. The effects of various disturbances, such as the carbody vibration [8,9], wind load [10–13], aerodynamics [14], dropper defect [15,16], contact wire irregularities [17] and contact wire height gradience [18] were included in the numerical simulation to predict the pantograph-catenary interaction performance. But the huge computational cost of numerical simulation is always a big concern for researchers in this field. This motivated different scholars to propose efficient simulation approaches [19,20] or reduced models [21] instead of using a full FE model of the catenary. To achieve the optimal design strategy, the genetic algorithm was implemented on a pantograph-catenary model with the help of a fast integration method for reducing the contact force standard deviation [22]. Based on the sensitivity analysis results, an optimisation strategy of the pantograph-catenary system was also proposed in Ref. [23]. Similar work was conducted *via* the combination of an artificial neural network and genetic algorithm on an existing pantograph-catenary system in the China high-speed railway network [24].

The rapid development of artificial intelligence techniques provides a new opportunity for developing a data-driven model of pantograph-catenary interaction. Deep learning, as a branch of neural network-based artificial intelligence, has demonstrated its potential in modelling complex systems with strong nonlinearity [25]. It has been widely used to handle the inherent nonlinearities in structural health monitoring of rail infrastructures [26–29] and traction power systems [30]. The application of deep learning for the surrogate modelling of the physical model can provide an alternative solution for predicting dynamic performance with almost no computational cost. The Long-Short-Term-Memory (LSTM) is a classic variant of the standard recurrent neural network architecture widely used in long-term time history prediction [31,32]. It has also exhibited excellent performance in building the surrogate model for complex objects [33,34].

1.3. Scope and contribution

This paper attempts to build a surrogate model of the physical pantograph-catenary model using deep learning and investigate its potential application in the optimisation of the design strategy. A FE model of the pantograph-catenary system that has been validated through a benchmark and field test data is presented to generate the training dataset. A deep neural network based on LSTM is proposed to capture the nonlinear relationship between the model parameters and the resulting contact force. The effectiveness of the proposed surrogate model is evaluated through several case studies, and the effect of neural network architecture on prediction performance is investigated. The potential of the proposed surrogate model in the optimisation of a pantograph-catenary system is explored.

2. Physical model of pantograph-catenary

In this work, a mature FE model of pantograph-catenary is adopted to generate the dataset for training the deep neural network. This model has been used in several previous works and has been demonstrated to have sufficient accuracy in approximating the realistic behaviours of pantograph-catenary interaction. Its numerical accuracy has been validated *via* the comparison with the

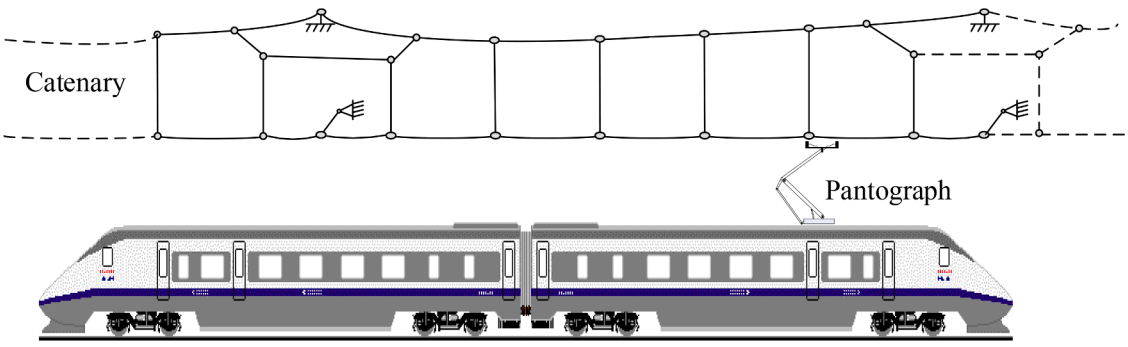

Fig. 1. Schematic of a pantograph-catenary system.

worldwide benchmark [35], the European standard [36], and the measurement data from both the Norwegian network [37] and the China high-speed railway network [38]. In this section, the pantograph-catenary model is briefly described as follows.

The catenary is modelled by the absolute nodal coordinate formulation (ANCF), as it can efficiently describe the geometric nonlinearity of the contact and messenger wires when large deformation occurs. As shown in Fig. 2, the ANCF beam element is used to discretise the contact and messenger wires. The dropper slackness is assumed by a cable element with nonlinear axial stiffness. The steady arm is assumed to be a truss element, which can rotate around the registration point. Claws and clamps are taken as additional lumped masses on the wire. The nodal degree of freedom vector of an ANCF beam element is defined as

$$\mathbf{e} = \left[x_i \quad y_i \quad z_i \quad \frac{\partial x_i}{\partial \chi} \quad \frac{\partial y_i}{\partial \chi} \quad \frac{\partial z_i}{\partial \chi} \quad x_j \quad y_j \quad z_j \quad \frac{\partial x_j}{\partial \chi} \quad \frac{\partial y_j}{\partial \chi} \quad \frac{\partial z_j}{\partial \chi} \right]^{\mathrm{T}} \tag{1}$$

where, χ is the local coordinate from 0 to the element length L_0. The strain energy from axial and bending deformation can be expressed by

$$U = \frac{1}{2}\int_0^{L_0} \left(EA\varepsilon_l^2 + EI\kappa^2 \right) d\chi \tag{2}$$

where, E is elastic modulus, A is the cross-section area, I is the inertial moment, ε_l is the longitudinal strain and κ is the curvature. By differentiating the strain energy, the generalised elastic force vector can be obtained as

$$\mathbf{Q} = \left(\frac{\partial U}{\partial \mathbf{e}} \right)^T = \mathbf{K}_e \mathbf{e} \tag{3}$$

The elastic forces can be written as the product of $\mathbf{K}_e$ and $\mathbf{e}$. $\mathbf{K}_e$ is the secant stiffness matrix as it is defined upon the absolute coordinate of the beam element. In the shape-fining process, the tangent stiffness matrix is more likely to be used to calculate the incremental nodal DOF vector $\Delta\mathbf{e}$ and the incremental unstrained length ΔL_0. The corresponding tangent stiffness matrices $\mathbf{K}_\mathrm{T}$ and $\mathbf{K}_\mathrm{L}$ can be obtained by taking part of $\mathbf{Q}$ with respect to $\mathbf{e}$ and L_0 as follows.

$$\Delta\mathbf{F} = \frac{\partial \mathbf{Q}}{\partial \mathbf{e}}\Delta\mathbf{e} + \frac{\partial \mathbf{Q}}{\partial L_0}\Delta L_0 = \mathbf{K}_\mathrm{T}\Delta\mathbf{e} + \mathbf{K}_\mathrm{L}\Delta L_0 \tag{4}$$

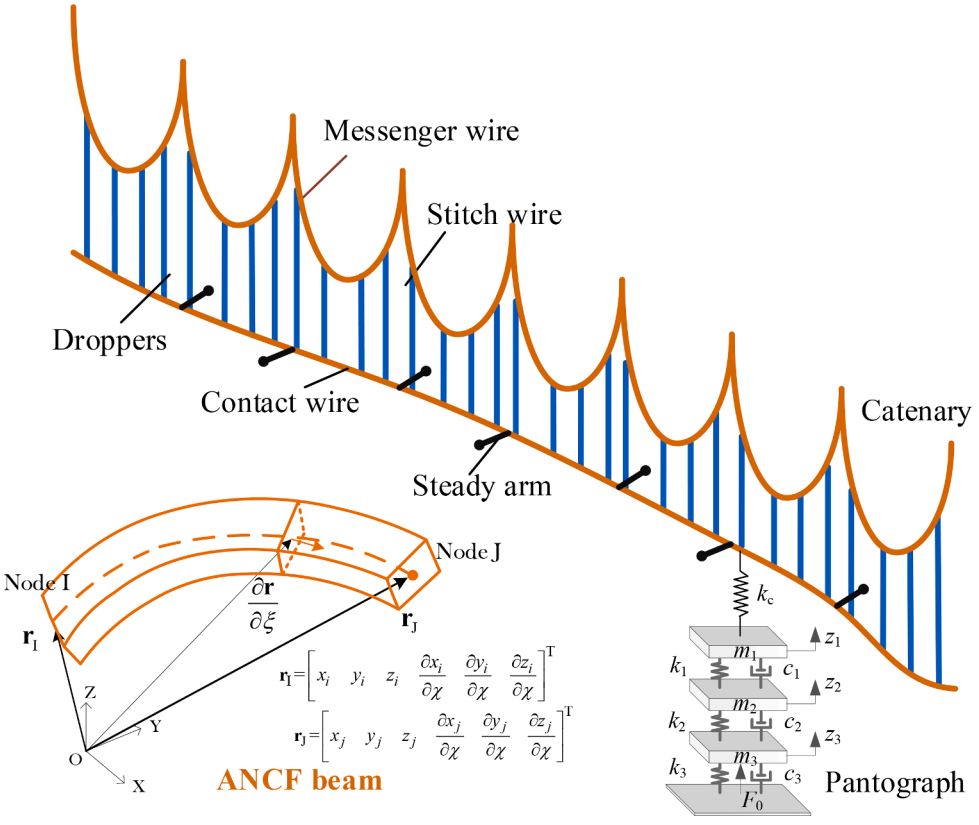

Fig. 2. Catenary model based on ANCF beam and cable elements. Red lines denote the ANCF beam element, and blue lines denote the ANCF cable element. (For interpretation of the references to colour in this figure legend, the reader is referred to the web version of this article.)

A similar derivation procedure can be used to obtain the tangent stiffness matrices of the ANCF cable elements. The cable elements used to model the dropper exhibit unsmooth nonlinearity due to dropper slackness in dynamic simulations, which changes the axial stiffness to zero when the dropper works in compression. Then a shape-finding procedure is adopted to compute the catenary configuration. The details about the shape-finding method can be seen in Ref. [39]. Then a consistent mass matrix and Rayleigh damping matrix are introduced to form the equation of motion for the catenary system, which can be written by

$$\mathbf{M}_{\mathrm{C}}^{\mathrm{G}}\ddot{\mathbf{U}}_{\mathrm{C}}(t)+\mathbf{C}_{\mathrm{C}}^{\mathrm{G}}\dot{\mathbf{U}}_{\mathrm{C}}(t)+\mathbf{K}_{\mathrm{C}}^{\mathrm{G}}(t)\mathbf{U}_{\mathrm{C}}(t)=\mathbf{F}_{\mathrm{C}}^{\mathrm{G}}(t) \tag{5}$$

in which $\mathbf{M}_{\mathrm{C}}^{\mathrm{G}}$, $\mathbf{C}_{\mathrm{C}}^{\mathrm{G}}$ and $\mathbf{K}_{\mathrm{C}}^{\mathrm{G}}$ are the mass, damping and stiffness matrix for the catenary system, respectively. The damping matrix $\mathbf{C}_{\mathrm{C}}^{\mathrm{G}}$ is given by the Rayleigh damping formulation [40,41]. $\mathbf{U}_{\mathrm{C}}(t)$ and $\mathbf{F}_{\mathrm{C}}^{\mathrm{G}}(t)$ are the DOF and external force vectors for the catenary system.

As illustrated in Fig. 2, the pantograph is assumed to be a lumped-mass representative of three critical modes of a realistic one. The vertical interaction of the panhead and the contact wire is described by the penalty function method. Based on the assumption of the relative penetration evaluated by vertical displacements of pantograph collector and contact wire, the contact force f_{c} can be calculated by

$$f_{\mathrm{c}}=\begin{cases} k_{\mathrm{s}}\delta & if\ \delta>0 \\ 0 & if\ \delta\le 0 \end{cases} \tag{6}$$

in which k_{s} is the contact stiffness, which should be a large value to avoid contaminating the frequency range of interest. The penetration δ is defined by the relative displacements of the panhead and the contact wire in the contact point.

3. Surrogate model

The proposed deep-learning approach for learning the surrogate model of the pantograph-catenary model is illustrated in Fig. 3. Generally, this approach takes the model parameters of pantograph-catenary interaction as the input for the FE model and a deep neural network based on LSTM. Through a number of dedicated numerical simulations, the FE model provides a tremendous amount of simulation data with different model parameters. These data are divided into training data and validation data. The training data are used to train the neural network to learn the inherent data dependencies between the input model parameters and the output contact force. The validation data are used to validate if the digital model can output the results with acceptable accuracy. In this section, the details of the neural network adopted to digitalise the pantograph-catenary model are described.

3.1. LSTM

For a typical forward neural network, the datasets flow from the input layer to the output layer. The error propagates backwards to modify the weights and biases to minimise the discrepancy between predicted results and training data [42]. Given an input matrix $\mathbf{X}=[x_1,x_2,\cdots,x_n]$, the output of hidden and output layers can be expressed by

$$\mathbf{h}=\mathrm{f}(\mathbf{U}\mathbf{X}+\mathbf{b}_1) \tag{7}$$

$$\mathbf{o}=\mathrm{g}(\mathbf{V}\mathbf{h}+\mathbf{b}_2) \tag{8}$$

where, $\mathbf{U}$ and $\mathbf{V}$ are the matrices connecting the input and hidden layers, hidden and output layers, respectively. $\mathbf{b}_1$ and $\mathbf{b}_2$ are the biases vectors in the input and hidden layers, respectively. f and g denote the activation functions in the hidden and output layers, respectively. In the traditional forward neural network, the prediction of current output is irrelevant to the previous information, and

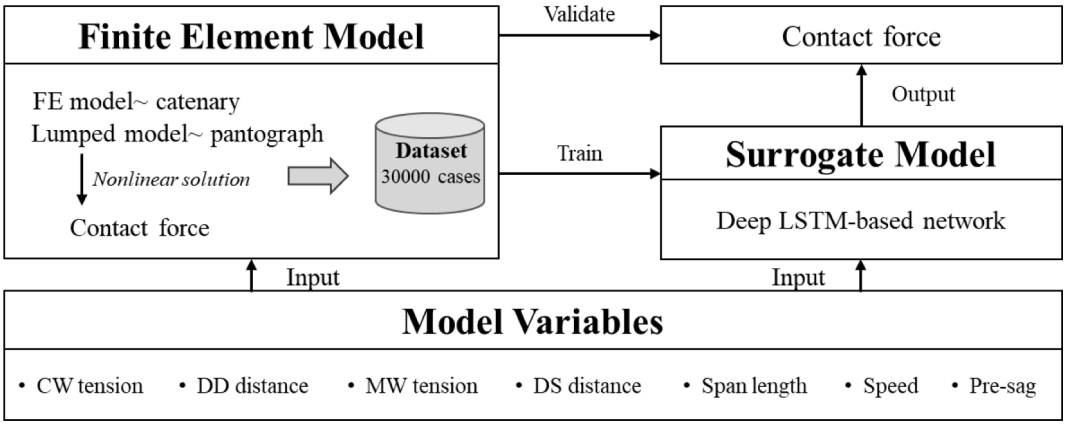

Fig. 3. Framework for the surrogate modelling.

its effect on the next-step prediction cannot be considered. To address this issue, the recurrent neural network (RNN) is developed, in which the prediction of output at the current step depends on both the current input parameters and the information transferred from the formerly hidden layer [44]. Compared with MLP (Multi-Layer Perceptron) and CNN (Convolutional Neural Networks), as shown in Table 1, RNN is more suitable for processing the time-series problem, such as time-series forecasting, natural language processing and sequential classification [43]. By including a weight matrix $\mathbf{W}$ connecting hidden layers at adjacent steps, Eq. (7) is modified to

$$\mathbf{h}^t = f\left(\mathbf{U}\mathbf{X} + \mathbf{W}\mathbf{h}^{t-1} + \mathbf{b}_1\right) \tag{9}$$

Unlike feedforward neural networks, RNNs have the advantage of history-dependent characteristics that is suitable to handle problems with sequential datasets. The output of a pantograph-catenary model, namely the pantograph-catenary contact force, is undoubtedly sequential by nature. LSTM network is a representative of RNN, which is easier to remember past data in memory without vanishing gradient problems [45]. As shown in Fig. 4, one cell of LSTM has three gates, namely, forget, input and output gates. Forget and input gates decide which information is discarded and stored from the memory cell. The output gate gives the ultimate output values. The outputs of forget and input gates at the tth step are obtained by

$$\mathbf{f}_j^t = \sigma\left(\left[\mathbf{U}_f\mathbf{X}^t\right]_j + \left[\mathbf{W}_f\mathbf{h}^{t-1}\right]_j + \left[\mathbf{b}_f\right]j\right) \tag{10}$$

$$\mathbf{i}_j^t = \sigma\left(\left[\mathbf{U}_i\mathbf{X}^t\right]_j + \left[\mathbf{W}_i\mathbf{h}^{t-1}\right]_j + \left[\mathbf{b}_i\right]_j\right) \tag{11}$$

in which σ is the sigmoid function. $\sigma = 1$ or 0 represents all information is kept or discarded, respectively. The memory cell state at the tth current step can be updated by

$$\widetilde{\mathbf{c}}_j^t = \tanh\left(\left[\mathbf{U}_c\mathbf{X}^t\right]_j + \left[\mathbf{W}_c\mathbf{h}^{t-1}\right] + \left[\mathbf{b}_c\right]_j\right) \tag{12}$$

$$\mathbf{c}^t = \mathbf{f}^t \odot \mathbf{c}^{t-1} + \mathbf{i}^t \odot \widetilde{\mathbf{c}}^t \tag{13}$$

where tanh is the activation function. $\odot$ is elementwise product. $\mathbf{f}^t \odot \mathbf{c}^{t-1}$ gives the discarded information. $\mathbf{i}^t \odot \widetilde{\mathbf{c}}^t$ denotes newly selected information. The updated memory cell status with an additional format can avoid the gradients vanishing and exploding. Thereafter, the output of the hidden layer at the tth step is obtained by

$$\mathbf{o}_j^t = \sigma\left(\left[\mathbf{U}_o\mathbf{X}_j^t\right]_j + \left[\mathbf{W}_o\mathbf{h}^{t-1}\right]_j + \left[\mathbf{b}_o\right]_j\right) \tag{14}$$

$$\mathbf{h}^t = \mathbf{o}^t \odot \tanh(\mathbf{c}^t) \tag{15}$$

3.2. Neural network architecture

The proposed network architecture is presented in Fig. 5. The network contains one input layer, one output layer, several LSTM layers and one fully connected layer, as shown in Fig. 5. A dropout layer with a dropout ratio of 0.3 is added after every LSTM layer to avoid overfitting. Note that the optimal number of LSTM layers is to be determined. For simplicity, Fig. 5 depicts the architecture with one LSTM layer and the corresponding dropout layer. The last dropout layer connects with the fully connected layer. This network's deep structure aims to capture the strong nonlinearity of the pantograph-catenary dynamics while preserving the network's ability to approximate pantograph-catenary simulations under various model parameters. As suggested in Refs. [46,47], after an LSTM layer, a fully connected (FC) layer is typically added to map the predicted sequence to the desired output size. It is noticed that the input size is 7, which is extended to a high dimension in the hidden layer. The function of the fully connected layer is to reduce the size of the hidden layer to the size of the output, which is only one dimension, contact force time history.

The main purpose of the surrogate model is to learn the complex nonlinear relationship between the main model parameters and the dynamic performance. According to EN 50367 [48], the main indicator to represent the current collection quality is the contact force filtered within 0–20 Hz, which is taken as the output in the neural network. The catenary with 15 spans is built in the FE model, and the contact forces in the central four spans are adopted to generate the dataset for training the neural network. The contact force is discretised into 600 points, which is sufficient to describe the dynamic characteristic within 20 Hz. The main six structural parameters of the catenary and the train speed are taken as the input model parameters as follows. Each of them is extended to the same dimension as the output contact force.

Table 1
Comparison of three types of neural networks [43].

Type of neural network	Main functions
MLP	The basic deep neural network. Most used for overcoming the high computing power of deep learning architecture.
CNN	Used in computer vision, e.g. image classification, face authentication and image semantic segmentation.
RNN	Used in time-series processing, e.g. time-series forecasting, natural language processing, and sequential classification.

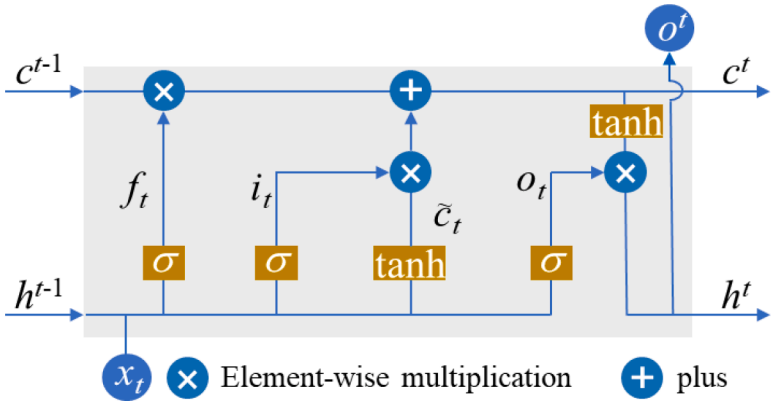

Fig. 4. Memory cell of LSTM.

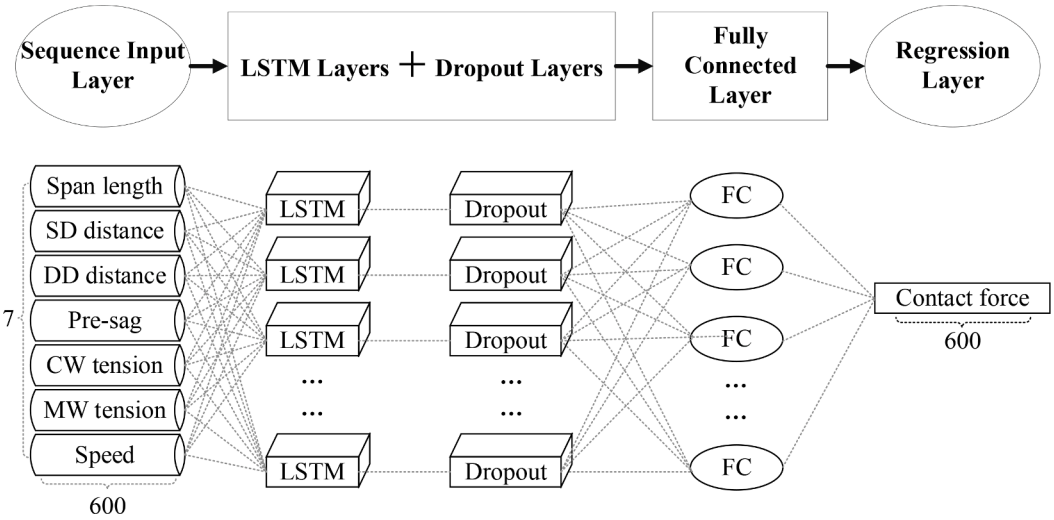

Fig. 5. Network architecture for the surrogate modelling of pantograph-catenary interaction.

- ***Geometry parameters:*** span length (L_s), steady arm-dropper distance (D_{sd}), dropper-dropper distance (D_{dd}), pre-sag (P_{sag})
- ***Tension parameters:*** contact wire tension (T_{cw}), messenger wire tension (T_{mw})
- ***Operation parameters:*** speed (v)

The potential of the surrogate model does not attempt to cover all the cases of pantograph-catenary systems in the world. Normally the optimisation of structural parameters is performed at a given speed [49]. Thus, a limited speed range is reasonable for generating the dataset. In this work, a high-speed range is considered, and the ranges of all the parameters are defined as follows according to the design specification [50].

Span length: 50 – 60 m; ***Steady arm-dropper distance:*** 4 – 6 m;
Dropper-dropper distance: 6 – 12 m; ***Pre-sag:*** 0 - 1.5‰;
Contact wire tension: 22,000 – 28,500 N;
Messenger wire tension: 17,000 – 23,000 N; ***Speed:*** 250 – 350 km/h;

It should be noted that the boundary of each parameter is extended a bit outside of the real value used in a realistic system in the world to represent the generality. For instance, the maximum contact wire tension used in the catenary without stitch wire is 27,000 N used in the Beijing-Tianjin high-speed line. This is extended up to 28,500 N in generating the dataset, which is helpful for the user to investigate the potential of the catenary with a higher tension class. Similarly, the pre-sag used in the current high-speed lines is no more than 1‰. This is extended up to 1.5‰ in generating the dataset.

To ensure the existence of the catenary geometry, the following constraint is applied:

$$\frac{L_s - 2D_{sd}}{D_{dd}} = \text{integer} \tag{16}$$

To avoid the exaggerated difference in the tensions of both messenger and contact wires, the following constraint is applied

$$|T_{\mathrm{cw}} - T_{\mathrm{mw}}| < 11000N \tag{17}$$

In the numerical simulation, a typical high-speed pantograph, WBL 85, is adopted, of which parameters can be seen in Ref. [37]. The mean contact force is regulated to the upper bound of the standard range specified in En 50367 [48], as assumed in many simulations [51,52]. The other parameters of the catenary, such as Young's modulus, and cross-section area of wires, refer to the Beijing–Tianjin passenger special line, which employs a typical high-speed catenary without stitch wires [9]. The catenary with 15 spans is adopted in the numerical simulation, and the statistical analysis is performed based on the resulting contact force in the central four spans. Based on the above-specified ranges of all model parameters, we randomly performed 30,000 cases of numerical simulation to set up a database for training and testing the proposed network. 80% of datasets are used to train the network, while the remaining 20% of datasets are used to test the network. The typical loss function, mean square error based on a 10-fold cross-validation method, is adopted to monitor the training performance.

$$MSE = \frac{1}{10r}\sum_{i=1}^{10}\sum_{j=1}^{r}\left(y_i^{\mathrm{s}} - y_i^{\mathrm{p}}\right)^2 \tag{18}$$

in which y_i^{s} is the simulated result obtained by the FE model at the ith point. y_i^{p} is the predicted result at the ith point. r is a total dataset in one cross-validation set. When training the neural network, the number of maximum epochs is chosen as 4000. The minimum batch size is defined as 256, and the initial learning rate is 0.0001. The replacement optimisation algorithm for stochastic gradient descent, Adam, is selected to train the model. Before training the neural network, all data are normalised according to their categories.

4. Performance evaluation of surrogate model

In this section, the performance of the proposed surrogate model is evaluated. Firstly, a neural network with hidden layers of '600 LSTMs + 400 LSTMs' is trained. Its accuracy in predicting the pantograph-catenary interaction performance is preliminarily analysed. Then, the performance is evaluated with different neural network architectures.

4.1. Preliminary analysis

Firstly, a neural network with hidden layers of two LSTM layers, '600 LSTMs + 400 LSTMs', is trained by the first 24,000 cases

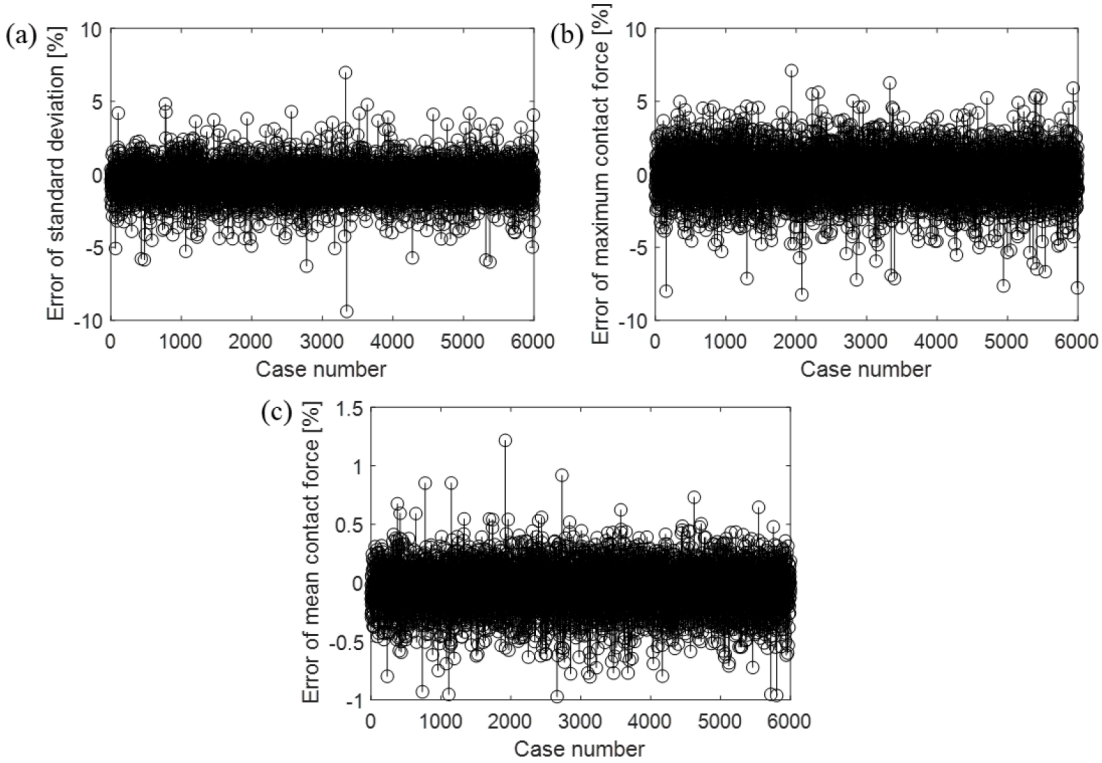

Fig. 6. Errors of the predicted contact force standard deviation (a), maximum contact force (b) and mean contact force (c) against the FEM results.

obtained by FE simulations. The last 6000 cases are used to check the accuracy of the prediction. The errors of the predicted contact forces' standard deviation, maximum value, and mean value against the FEM results are presented in Fig. 6. Note that the surrogate model only takes no more than 0.4 s to compute the contact forces in each case which costs more than 1200s in traditional FEM simulation. According to En 50367 [48], the contact force standard deviation is the most important indicator to represent the current collection quality. It is seen from Fig. 6(a) that 99.70% of the predicted results have an error of less than 5%. The maximum error of the standard deviation reaches 9.393%. According to the benchmark results [7], the contact force standard deviations evaluated by ten mainstream software have a deviation of up to 15.4%. Thus, it can be inferred that the results predicted by the surrogate model have acceptable accuracy. Speaking of the maximum contact force shown in Fig. 6(b), 99.48% of the predicted results have an error of less than 5%. As shown in Fig. 6(c), the mean contact forces evaluated by the surrogate model do not have significant errors against the FEM results.

It is also seen from Fig. 6(a) that the maximum error of contact force standard deviation occurs in case 3346. The contact force evaluated by both the surrogate model and FE model in this 'worst case' is presented in Fig. 7. It is seen that even in such a case, a good agreement can still be observed from the contact forces, which further demonstrates the acceptance of the proposed surrogate model.

To statistically analyse the prediction error, the histograms of the prediction error of contact force standard deviation, maximum contact force, and mean contact force are presented in Fig. 8. It is seen that the prediction errors generally follow the normal distribution. In most engineering applications, three-sigma limits are used to set the upper and lower control limits in a statistical quality control [53], which means that 99.73% of data observed following a normal distribution lies within three standard deviations of the mean. In physics, a more strict criterion of 5 standard deviations is more likely to be used, which ensures an almost 100% (99.99994%) confidence. In this analysis, both confidence levels are plotted. As for the contact force standard deviation in Fig. 8(a), 99.73% of prediction errors are no more than 3.67%, while almost 100% of cases have an error lower than 5.75%. For the maximum contact force in Fig. 8(b), it is seen that 99.73% of prediction errors are no more than 4.56%, while almost 100% of cases have an error lower than 7.53%. For the mean contact force in Fig. 8(c), almost 100% of cases have an error lower than 1%.

The previous analyses in Refs. [22,54,55] demonstrate the strong nonlinearity of the pantograph-catenary system, and the response does not show a simple change in the system parameters. Even in Ref. [24], the neural network is used to learn a pantograph-catenary model, but the output is only the contact force statistics instead of the contact force time history.

To further demonstrate the necessity of using a complex deep learning network, a simple regression (linear regression) method is implemented to represent the pantograph-catenary model with the given database. Note that the regression method can only output the contact force statistics (the standard deviation, the maximum contact force and the mean contact force), but not the contact force time history. The linear regression can be expressed as follows:

$$\eta = \sum_{n=1}^{7} b_n v_n \tag{19}$$

in which η is the output of the linear regression, which is the standard deviation, the maximum contact force or the mean contact force. v1-v7 are the variables, namely the span length, steady arm-dropper distance, dropper-dropper distance, pre-sag, contact wire tension, messenger wire tension and speed. $b1$-$b6$ are the corresponding weight for each variable, respectively. A total of 30,000 cases are used here to build the regression model. The obtained weights are shown as follows:

- For the standard deviation, $b1$-$b6$ are -0.8709, -2.3867, 0.687, 2.9888×10^{4}, -8.7658×10^{-4} -2.9179×10^{-4}, and 1.3530, respectively.
- For the maximum contact force, $b1$-$b6$ are -1.7817, 5.0639, 1.4595, 6.2805×10^{4}, -0.0047, -0.001, and 5.1682, respectively.
- For the mean contact force, $b1$-$b6$ are -0.1035, -0.5288, -0.1265, -1.3122×10^{3}, -2.1251×10^{-5}, -1.9985×10^{-4}, and 2.0823, respectively.

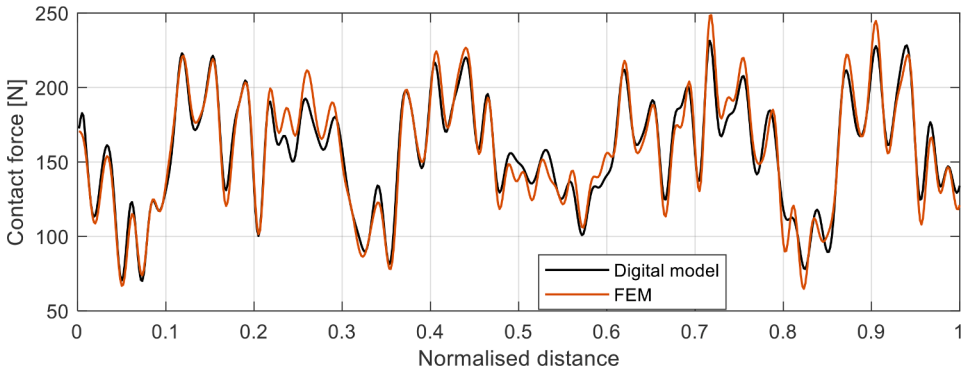

Fig. 7. The comparison of contact force simulated by the surrogate model and the FE model. This is the worst case that has the largest prediction error in the contact force standard deviation.

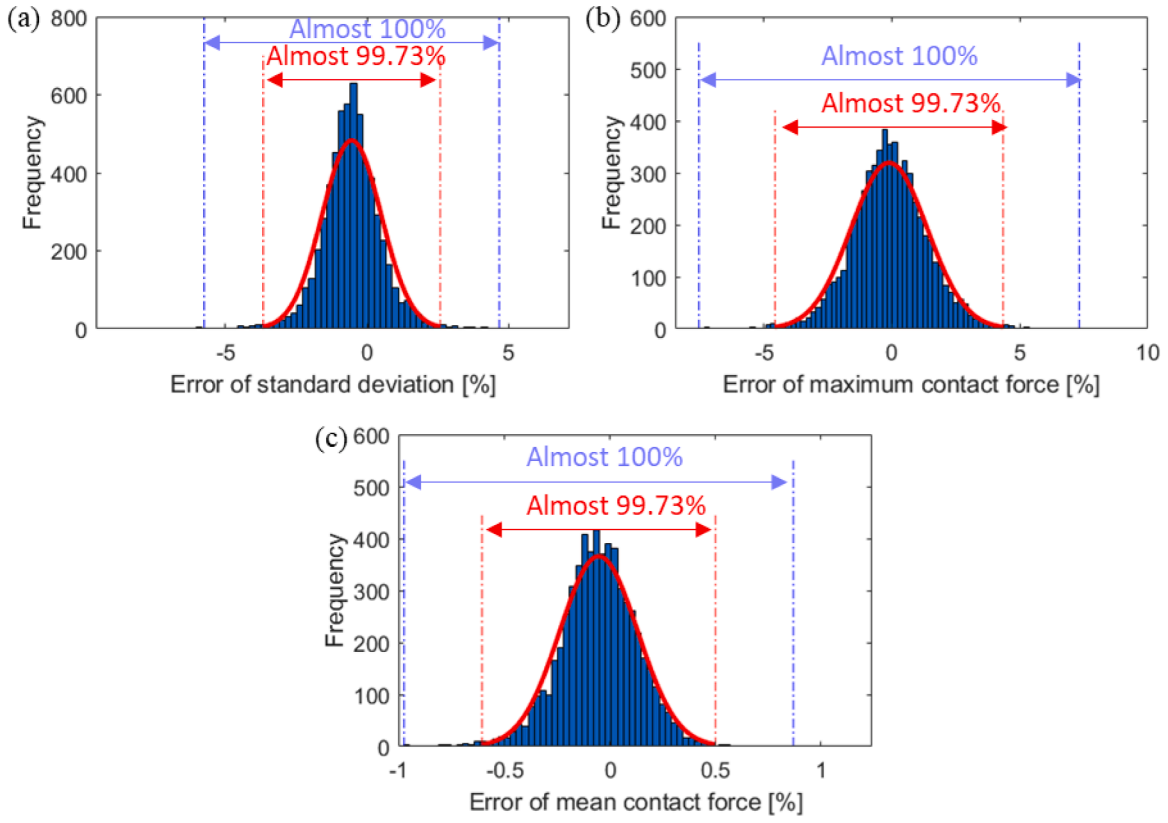

Fig. 8. Histograms of the prediction error of contact force standard deviation (a), maximum contact force (b) and mean contact force (c) against the FEM results.

The errors of contact force statistics evaluated by the linear regression model against the FEM results are presented in Fig. 9. It is seen that the maximum errors of the maximum contact force, contact force standard deviation and mean contact force reach over 20%, 50% and 2%, respectively. The prediction performance of the linear regression model is significantly unacceptable. This finding is consistent with the common sense that the pantograph-catenary system has strong nonlinearity and cannot be represented or learned by a simple linear model.

4.2. Different network architectures

In this section, the effect of network architecture on prediction performance is investigated. Determining the neural network architecture is a very complex topic, which is relevant to the complexity of the problem, the data dimension, the computational capacity and other factors. Normally the neural network's architecture is determined by experience and understanding of the addressed problem. For the pantograph-catenary system discussed in this paper, some very simple network architectures that only contain dozens of LSTM neurons are tested, but they lead to unacceptable performance, which is consistent with our expectation of a strongly nonlinear system. Some very complicated architectures with thousands of LSTM neurons are also tested, but they are significantly above the computational capacity of a common work computer and unnecessarily complicated as proven later. With the above consideration, seven neural network architectures are defined in Table 2. NN 5 is the network analysed in Section 4.1. From NN 1 to NN 6, the network architecture becomes more complex in terms of the number of layers and neurons. NN 7 is obtained by slightly adjusting the layers' sequence of NN 6.

Each of the above networks is trained by 24,000 cases of the FEM result, and the 6000 cases are used to validate the prediction accuracy. The mean and maximum errors of predicted contact force statistics against FEM results are presented in Fig. 10(a) and (b), respectively. It is seen that amongst the first five NNs, the NN 5 generally has the best prediction performance. A general trend can be observed that the increase in the network architecture complexity leads to increased prediction accuracy. The prediction performance of NNs 3, 4 and 5 generally does not exhibit a significant variance. When the network architecture complexity reaches a certain level (in terms of the number of layers and neurons), the adjustment of the network architecture will no longer primarily affect the prediction accuracy. However, a too-complex architecture, such as NNs 6 and 7, may degrade the prediction performance. This may be caused by difficulties in convergence or overfitting when too-complex architectures are used. Normally, the determination of a neural network architecture should depend on the dataset's capacity and the task's complexity [56]. In this study, NNs 3–5 show a good performance with the given dataset of 30,000 cases.

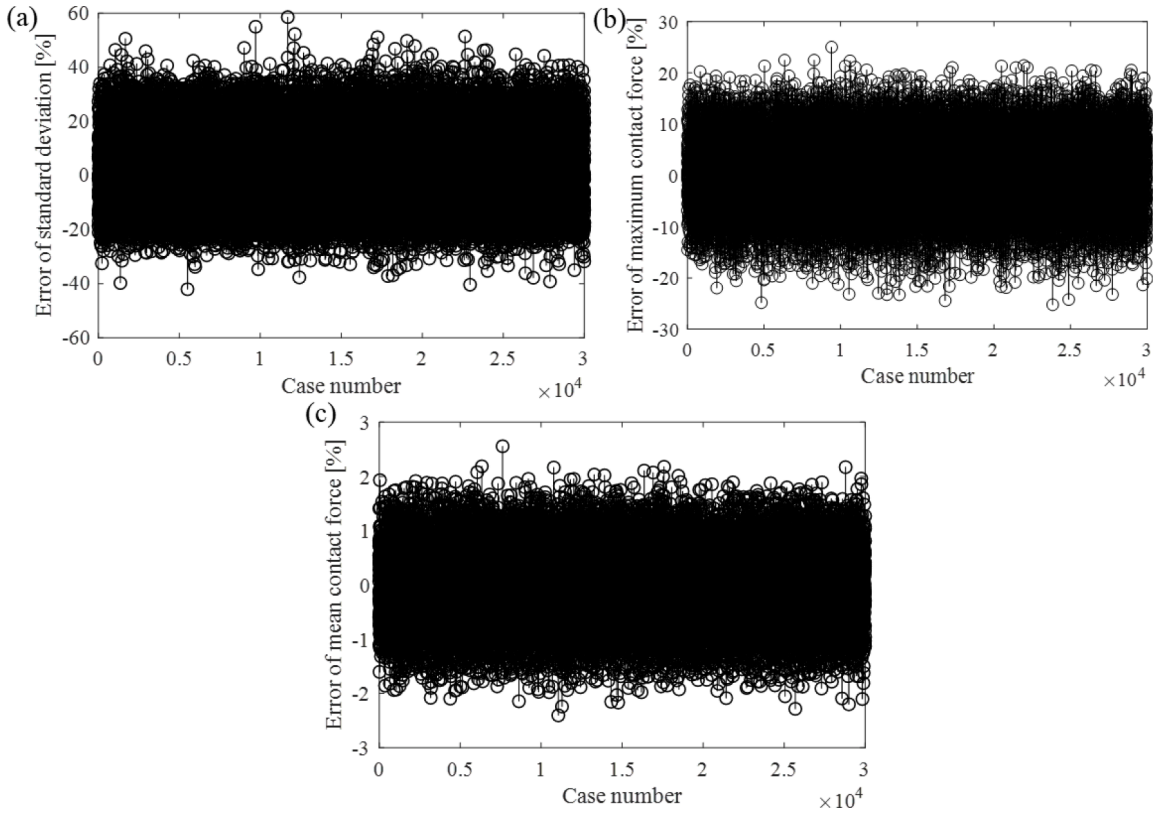

Fig. 9. Errors of the contact force statistics (standard deviation (a), maximum contact force (b), and mean contact force (c)) predicted by the regression model against the FEM results.

Table 2
Architectures of LSTM layers.

Network No.	Architecture of LSTM layers
NN1	200 LSTMs
NN2	400 LSTMs
NN3	400 LSTMs + 200 LSTMs
NN4	600 LSTMs
NN5	600 LSTMs + 300 LSTMs
NN6	600 LSTMs + 300 LSTMs + 150 LSTMs
NN7	300 LSTMs + 600 LSTMs + 300 LSTMs

Due to the implementation of the stochastic gradient descent method in the training process [57], the prediction performance of a neural network may vary amongst multiple times of training even if the architecture remains the same. Taking NN 5 as an example, the mean and maximum prediction errors with four times of training are presented in Fig. 11(a) and (b), respectively. Even though the same NN architecture and parameter setup is adopted four times for training, NN 5 exhibits different prediction accuracy. Amongst the four times of training, the mean error of the contact force standard deviation varies from 0.79% to 1.03%, while the maximum error varies from 8.22% to 11.10%. The 3rd training of the NN 5 has the best perdition accuracy, which is adopted to perform the subsequent analysis.

5. Potential application in catenary optimisation

This section discusses the potential of the surrogate model in catenary design optimisation. A genetic algorithm method is used to obtain the optimal structure of the catenary under given constraints. Normally the design speed and the tension class for a catenary are determined before the optimisation is performed. The former depends on the rail network's commercial demand, while the latter is determined by the limitation of wave speed and material property [54]. Here we present two cases as follows based on practical experience. To save the economic cost of construction, a long span length is normally preferred [50]. Therefore, the span length is also restricted to the upper bound of the specified range of 60 m.

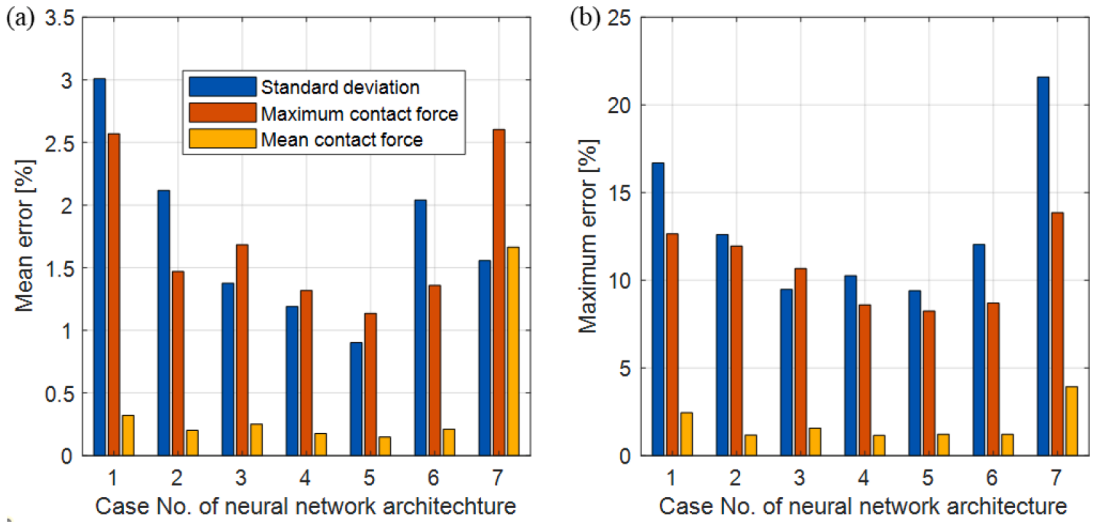

Fig. 10. Mean (a) and maximum (b) errors of predicted contact force statistics against FEM results.

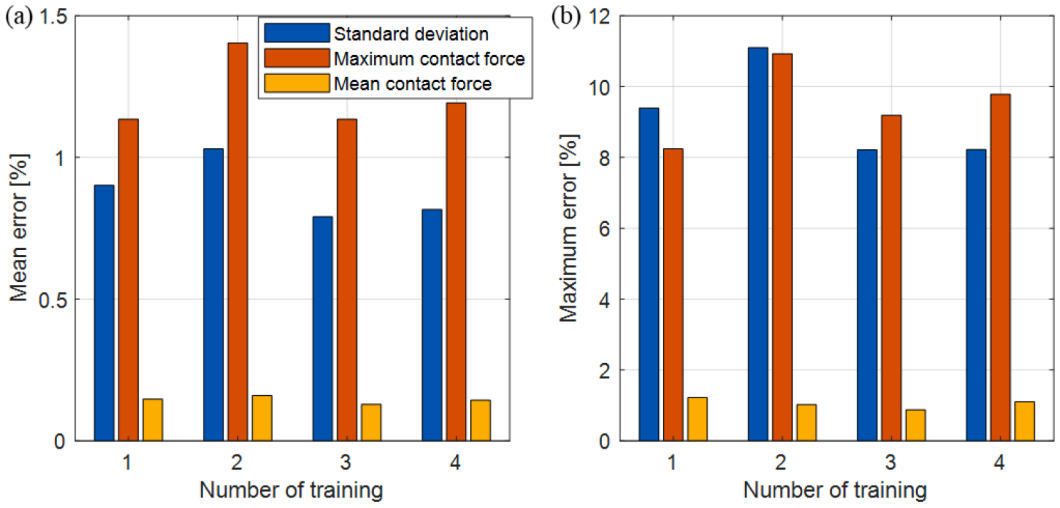

Fig. 11. Mean (a) and maximum (b) prediction errors of NN 5 with 4 times of training.

Case 1: $v = 350$; $T_{cw} = 27$ kN; $L_s = 60$ m
Case 2: $v = 320$; $T_{cw} = 23$ kN; $L_s = 60$ m

In each case, v, T_{CW} and L_s are constrained, and other parameters D_{sd}, D_{dd}, P_{sag} and T_{mw} are taken as the variables that are desired to be optimised. The objective function is to minimise the standard deviation of the contact force. Thus, the optimisation problem reads:

$$\text{Objective}: \min \sigma\left(f_c\left(L_s, D_{sd}, D_{dd}, P_{sag}, T_{mw}, T_{cw}, v\right)\right)$$

$$\text{Boundary constraints}: 4 \le D_{sd} \le 6\text{m}\, 6 \le D_{dd} \le 12\text{m}$$

$$0 \le P_{sag} \le 1.5\%;\ 17000 \le T_{mw} \le 23000\text{N}$$

Design constraints: v = specified value; T_{cw} = specified value; L_s = specified value
Other constraints: Eqs. (16) and (17)

Then the genetic algorithm is implemented to solve the optimisation problem. Fig. 12 shows the optimisation results of case 1. It can be seen from Fig. 12(a) that the best optimal result is achieved after 158 iterations. The optimised parameters for case 1 are $D_{sd} =$ 5.99 m; $D_{dd} = 9.60$ m, $P_{sag} = 0.10325‰$; $T_{mw} = 18{,}198.36$ N, and the optimised contact force standard deviation is 43.94 N. It only takes 692.53 s to finalise the optimisation for this case, which is several days of work when using the traditional FE model. The comparison with 10,000 randomly generated case results is presented in Fig. 12(b) to verify the optimised result further. The optimisation results of case 2 are presented in Fig. 13. The optimised parameters for case 2 are $D_{sd} = 5.6461$ m; $D_{dd} = 8.1181$ m, $P_{sag} =$

0.15667‰; $T_{mw} = 21{,}185.46$ N, and the optimised contact force standard deviation is 36.21 N. It only takes 692.53 s to achieve the best result. Similarly, the effectiveness of the optimisation result can be demonstrated by comparison with 10 000 randomly generated case results, as presented in Fig. 13(b).

6. Conclusions and future works

In this study, a surrogate model based on the LSTM neural network is proposed to approximate a FE model of railway pantograph-catenary systems. The presented results indicate that the contact forces predicted by the surrogate model and FEM have a good agreement. The computational effort of the surrogate model can be neglected compared with FEM. The statistical analysis points out that almost all the predictions have an error of less than 5.75% in terms of the contact force standard deviation. The optimal neural network architecture of the surrogate model can be determined when increasing the architecture complexity does not guarantee a higher prediction accuracy. The utilisation of the stochastic gradient descent method leads to stochasticity in the network's prediction performance amongst multiple times of training with the same network architecture. Through two optimisation cases, it is demonstrated that the proposed surrogate model can effectively accelerate the optimization of catenary structural parameters with the help of a genetic algorithm. In the future, more potential applications of the present surrogate model of the pantograph-catenary system will be explored for the life cycle management of the railway infrastructure.

Note that this paper only presents the surrogate modelling of a pantograph-catenary model with specific parameters. There are several angles to be considered in future works. The first is to improve the generality of the present model to cover more variety of pantograph-catenary systems. The second is to include measurement data to establish the relationship between the design parameters and field test data, which makes the predictions more realistic and potentially useful for maintenance decision-making. The last is to investigate the possibility of developing a neural network-based optimisation algorithm with more advanced objectives for the pantograph-catenary system. Also, in light of the excellent prediction performance in the presented case study, a surrogate model may be trained to achieve real-time simulations in Hardware-in-The-Loop test rigs by adjusting the training strategy.

Declaration of Competing Interest

The authors declare the following financial interests/personal relationships which may be considered as potential competing interests:

Yang Song, Zhigang Liu reports financial support was provided by National Natural Science Foundation of China. Yang Song, Gunnstein Froseth, Petter Navik, Anders Ronnquist reports financial support was provided by Norwegian Railway Directorate.

Data availability

The authors do not have permission to share data.

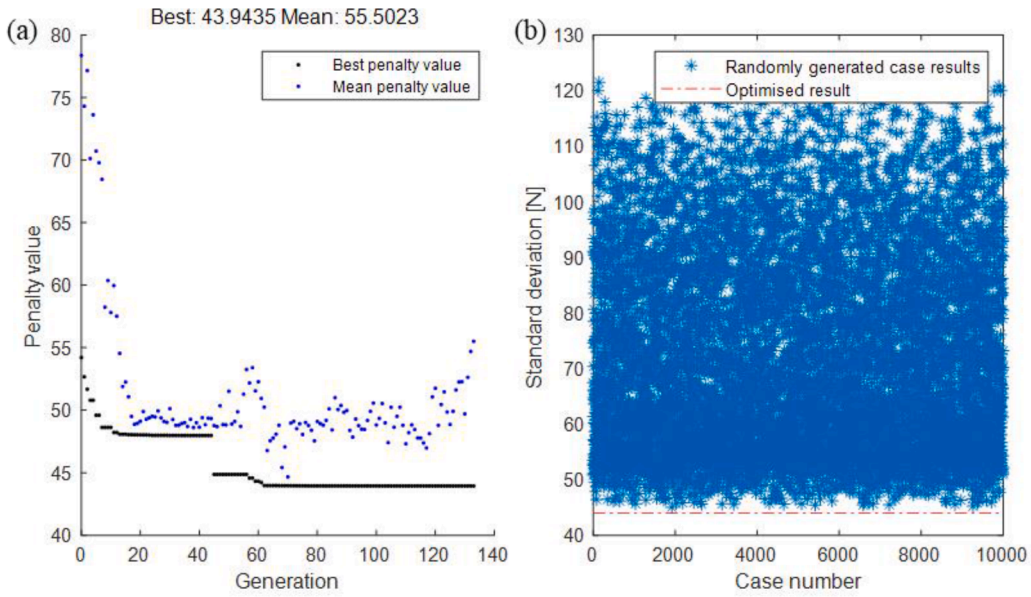

Fig. 12. Optimisation of case 1. Penalty value versus generation (a). Comparison with 10,000 randomly generated case results (b).

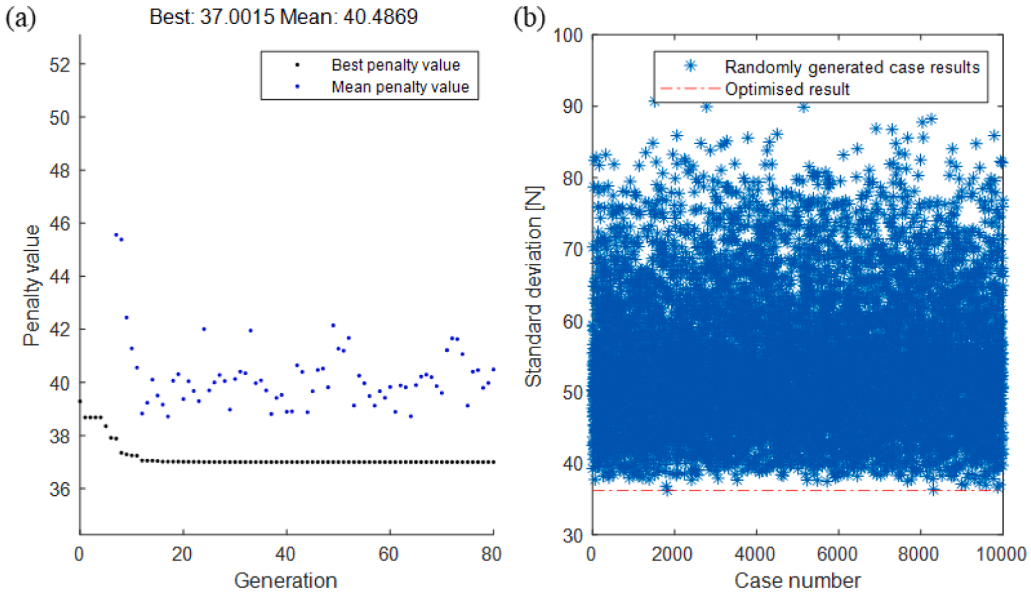

Fig. 13. Optimisation of case 2. Penalty value versus generation (a). Comparison with 10,000 randomly generated case results (b).

Acknowledgments

The work presented in this paper is funded by National Natural Science Foundation of China (5217120182) and the Norwegian Railway Directorate.

References

[1] S. Bruni, G. Bucca, M. Carnevale, A. Collina, A. Facchinetti, Pantograph–catenary interaction: recent achievements and future research challenges, Int. J. Rail Transp. 6 (2) (2018) 57–82, https://doi.org/10.1080/23248378.2017.1400156.
[2] W. Zhang, D. Zou, M. Tan, N. Zhou, R. Li, G. Mei, Review of pantograph and catenary interaction, Front. Mech. Eng. 13 (2) (2018) 311–322, https://doi.org/10.1007/s11465-018-0494-x.
[3] Y. Ye, P. Huang, Y. Sun, D. Shi, MBSNet: a deep learning model for multibody dynamics simulation and its application to a vehicle-track system, Mech. Syst. Signal Process. 157 (2021), 107716, https://doi.org/10.1016/j.ymssp.2021.107716.
[4] J. Nespoulous, C. Soize, C. Funfschilling, G. Perrin, Optimisation of train speed to limit energy consumption, Veh. Syst. Dyn. (2021), https://doi.org/10.1080/00423114.2021.1965628.
[5] H. Chen, B. Jiang, S.X. Ding, B. Huang, Data-driven fault diagnosis for traction systems in high-speed trains: a survey, challenges, and perspectives, IEEE Trans. Intell. Transp. Syst. (2020) 1–17, https://doi.org/10.1109/tits.2020.3029946.
[6] A. Cozad, N.v. Sahinidis, D.C. Miller, Learning surrogate models for simulation-based optimization, AIChE J. 60 (6) (2014) 2211–2227, https://doi.org/10.1002/aic.14418.
[7] S. Bruni, et al., The results of the pantograph-catenary interaction benchmark, Veh. Syst. Dyn. 53 (3) (2015) 412–435, https://doi.org/10.1080/00423114.2014.953183.
[8] Y. Yao, D. Zou, N. Zhou, G. Mei, J. Wang, W. Zhang, A study on the mechanism of vehicle body vibration affecting the dynamic interaction in the pantograph–catenary system, Veh. Syst. Dyn. 59 (9) (2021) 1335–1354, https://doi.org/10.1080/00423114.2020.1752922.
[9] Y. Song, Z. Wang, Z. Liu, R. Wang, A spatial coupling model to study dynamic performance of pantograph-catenary with vehicle-track excitation, Mech. Syst. Signal Process. 151 (2021), 107336, https://doi.org/10.1016/j.ymssp.2020.107336.
[10] Y. Song, F. Duan, S. Gao, F. Wu, Z. Liu, Crosswind effects on current collection quality of railway pantograph-catenary: a case study in chengdu-chongqing passenger special line, IEEE Trans. Instrum. Meas. (2021), https://doi.org/10.1109/tim.2021.3139661, 1–1.
[11] Y. Song, M. Zhang, O. Øiseth, A. Rønnquist, Wind deflection analysis of railway catenary under crosswind based on nonlinear finite element model and wind tunnel test, Mech. Mach. Theory 168 (2021) 2022, https://doi.org/10.1016/j.mechmachtheory.2021.104608.
[12] Y. Song, M. Zhang, H. Wang, A response spectrum analysis of wind deflection in railway overhead contact lines using pseudo-excitation method, IEEE Trans. Veh. Technol. 70 (2) (2021) 1169–1178, https://doi.org/10.1109/TVT.2021.3054459.
[13] F. Duan, et al., Study on aerodynamic instability and galloping response of rail overhead contact line based on wind tunnel tests, IEEE Trans. Veh. Technol. (2023), https://doi.org/10.1109/TVT.2023.3243024.
[14] Z. Dai, T. Li, J. Deng, N. Zhou, W. Zhang, Effect of the strip spacing on the aerodynamic performance of a high-speed double-strip pantograph, Veh. Syst. Dyn. (2021) 1–17, https://doi.org/10.1080/00423114.2021.1945117.
[15] Y. Song, Z. Liu, X. Lu, Dynamic performance of high-speed railway overhead contact line interacting with pantograph considering local Dropper Defect, IEEE Trans. Veh. Technol. 69 (6) (2020) 5958–5967, https://doi.org/10.1109/TVT.2020.2984060.
[16] F. Vesali, M.A. Rezvani, H. Molatefi, M. Hecht, Static form-finding of normal and defective catenaries based on the analytical exact solution of the tensile Euler–Bernoulli beam, Proc. Inst. Mech. Eng. F. J. Rail. Rapid Transit. 233 (7) (2019) 691–700, https://doi.org/10.1177/0954409718808990.
[17] Y. Song, Z. Liu, A. Ronnquist, P. Navik, Z. Liu, Contact wire irregularity stochastics and effect on high-speed railway pantograph-catenary interactions, IEEE Trans. Instrum. Meas. 69 (10) (2020) 8196–8206, https://doi.org/10.1109/TIM.2020.2987457.
[18] S. Hayes, D.I. Fletcher, A.E. Beagles, K. Chan, Effect of contact wire gradient on the dynamic performance of the catenary pantograph system, Veh. Syst. Dyn. 0 (0) (2020) 1–23, https://doi.org/10.1080/00423114.2020.1798473.
[19] S. Gregori, M. Tur, E. Nadal, J.v. Aguado, F.J. Fuenmayor, F. Chinesta, Fast simulation of the pantograph–catenary dynamic interaction, Finite Elem. Anal. Des. 129 (2017) 1–13, https://doi.org/10.1016/j.finel.2017.01.007.

[20] Y. Song, Z. Liu, Z. Xu, J. Zhang, Developed moving mesh method for high-speed railway pantograph-catenary interaction based on nonlinear finite element procedure, Int. J. Rail Transp. 7 (3) (2019) 173–190, https://doi.org/10.1080/23248378.2018.1532330.
[21] J. Gil, S. Gregori, M. Tur, F.J. Fuenmayor, Analytical model of the pantograph–catenary dynamic interaction and comparison with numerical simulations, Veh. Syst. Dyn. (2020) 1–24, https://doi.org/10.1080/00423114.2020.1802493.
[22] S. Gregori, M. Tur, E. Nadal, F.J. Fuenmayor, An approach to geometric optimisation of railway catenaries, Veh. Syst. Dyn. 56 (8) (2018) 1162–1186, https://doi.org/10.1080/00423114.2017.1407434.
[23] J. Zhang, W. Liu, Z. Zhang, Sensitivity analysis and research on optimisation methods of design parameters of high-speed railway catenary, IET Electr. Syst. Transp. 9 (3) (2019) 150–156, https://doi.org/10.1049/iet-est.2018.5007.
[24] K. Su, J. Zhang, J. Zhang, T. Yan, G. Mei, Optimisation of current collection quality of high-speed pantograph-catenary system using the combination of artificial neural network and genetic algorithm, Veh. Syst. Dyn. (2022), https://doi.org/10.1080/00423114.2022.2045029.
[25] B. Lusch, J.N. Kutz, S.L. Brunton, Deep learning for universal linear embeddings of nonlinear dynamics, Nat. Commun. 9 (1) (2018) 1–10, https://doi.org/10.1038/s41467-018-07210-0.
[26] Y. Ye, B. Zhu, P. Huang, B. Peng, OORNet: a deep learning model for on-board condition monitoring and fault diagnosis of out-of-round wheels of high-speed trains, Measurement (London) 199 (2022), 111268, https://doi.org/10.1016/j.measurement.2022.111268.
[27] Z. Wang, J. Xuan, T. Shi, Multi-source information fusion deep self-attention reinforcement learning framework for multi-label compound fault recognition, Mech. Mach. Theory 179 (2023), 105090, https://doi.org/10.1016/J.MECHMACHTHEORY.2022.105090.
[28] Z. Chen, J. Wu, C. Deng, C. Wang, Y. Wang, Residual deep subdomain adaptation network: a new method for intelligent fault diagnosis of bearings across multiple domains, Mech. Mach. Theory 169 (2022) 104635, https://doi.org/10.1016/j.mechmachtheory.2021.104635.
[29] D.S. Alves, et al., Uncertainty quantification in deep convolutional neural network diagnostics of journal bearings with ovalization fault, Mech. Mach. Theory 149 (2020), 103835, https://doi.org/10.1016/J.MECHMACHTHEORY.2020.103835.
[30] S. Gao, Automatic detection and monitoring system of pantograph-catenary in China's high-speed railways, IEEE Trans. Instrum. Meas. 70 (2021), https://doi.org/10.1109/TIM.2020.3022487.
[31] X. Li, L. Cao, A. Tiong, P.T. Phan, S.J. Phee, Distal-end force prediction of tendon-sheath mechanisms for flexible endoscopic surgical robots using deep learning, Mech. Mach. Theory 134 (2019) 323–337, https://doi.org/10.1016/j.mechmachtheory.2018.12.035.
[32] X. Li, H. Jiang, X. Xiong, H. Shao, Rolling bearing health prognosis using a modified health index based hierarchical gated recurrent unit network, Mech. Mach. Theory 133 (2019) 229–249, https://doi.org/10.1016/j.mechmachtheory.2018.11.005.
[33] M. Tang, Y. Liu, L.J. Durlofsky, A deep-learning-based surrogate model for data assimilation in dynamic subsurface flow problems, J. Comput. Phys. 413 (2020), 109456, https://doi.org/10.1016/J.JCP.2020.109456.
[34] Y. Zhang, S. Wang, G. Sun, J. Mao, Aerodynamic surrogate model based on deep long short-term memory network: an application on high-lift device control, Proc. Inst. Mech. Eng. G. J. Aerosp. Eng. 0 (0) (2021) 1–17, https://doi.org/10.1177/09544100211027023.
[35] Y. Song, A. Rønnquist, P. Nåvik, Assessment of the high-frequency response in railway pantograph-catenary interaction based on numerical simulation, IEEE Trans. Veh. Technol. 69 (10) (2020) 10596–10605, https://doi.org/10.1109/TVT.2020.3015044.
[36] Z. Xu, Y. Song, Z. Liu, Effective measures to improve current collection quality for double pantographs and catenary based on wave propagation analysis, IEEE Trans. Veh. Technol. 69 (6) (2020) 6299–6309, https://doi.org/10.1109/TVT.2020.2985382.
[37] Y. Song, A. Rønnquist, T. Jiang, P. Nåvik, Identification of short-wavelength contact wire irregularities in electrified railway pantograph–catenary system, Mech. Mach. Theory 162 (2021), 104338, https://doi.org/10.1016/j.mechmachtheory.2021.104338.
[38] J. Yang, Y. Song, X. Lu, F. Duan, Z. Liu, K. Chen, Validation and analysis on numerical response of super-high-speed railway pantograph-catenary interaction based on experimental test, Shock Vib. 2021 (2021) 1–13, https://doi.org/10.1155/2021/9922404.
[39] Y. Song, A. Rønnquist, T. Jiang, P. Nåvik, Railway pantograph-catenary interaction performance in an overlap section: modelling, validation and analysis, J. Sound Vib. 548 (2023), 117506, https://doi.org/10.1016/J.JSV.2022.117506.
[40] D. Zou, W.H. Zhang, R.P. Li, N. Zhou, G.M. Mei, Determining damping characteristics of railway-overhead-wire system for finite-element analysis, Veh. Syst. Dyn. 54 (7) (2016) 902–917, https://doi.org/10.1080/00423114.2016.1172715.
[41] L. Zhang, Z. Wang, Q. Wang, J. Mo, J. Feng, K. Wang, The effect of wheel polygonal wear on temperature and vibration characteristics of a high-speed train braking system, Mech. Syst. Signal Process. 186 (2023), 109864, https://doi.org/10.1016/J.YMSSP.2022.109864.
[42] Y. Yu, X. Si, C. Hu, J. Zhang, A review of recurrent neural networks: LSTM cells and network architectures, Neural Comput. 31 (7) (2019) 1235–1270, https://doi.org/10.1162/NECO_A_01199.
[43] P. Kim, Matlab deep learning with machine learning, neural networks and artificial intelligence, Apress (2017), https://doi.org/10.1007/978-1-4842-2845-6.
[44] A.C. Tsoi, Recurrent neural network architectures: an overview. Lecture Notes in Computer Science, Springer, Berlin, Heidelberg, 1998, pp. 1–26, https://doi.org/10.1007/bfb0053993.
[45] A. Sherstinsky, Fundamentals of Recurrent Neural Network (RNN) and Long Short-Term Memory (LSTM) network, Phys. D 404 (2020), 132306, https://doi.org/10.1016/j.physd.2019.132306.
[46] T.N. Sainath, O. Vinyals, A. Senior, H. Sak, Convolutional, long short-term memory, fully connected deep neural networks, in: ICASSP, IEEE International Conference on Acoustics, Speech and Signal Processing - Proceedings 2015, 2015, pp. 4580–4584, https://doi.org/10.1109/ICASSP.2015.7178838.
[47] Z. Zhang, Z. Lv, C. Gan, Q. Zhu, Human action recognition using convolutional LSTM and fully-connected LSTM with different attentions, Neurocomputing 410 (2020) 304–316, https://doi.org/10.1016/j.neucom.2020.06.032.
[48] European Committee for Electrotechnical Standardization, EN 50367. Railway Applications — Current collection Systems — Technical criteria For the Interaction Between Pantograph and Overhead Line, European Standards (EN), Brussels, 2016.
[49] J. Ambrósio, J. Pombo, M. Pereira, Optimization of high-speed railway pantographs for improving pantograph-catenary contact, Theor. Appl. Mech. Lett. 3 (1) (2013), 013006, https://doi.org/10.1063/2.1301306.
[50] F. Kiessling, R. Puschmann, A. Schmieder, E. Schneider, Contact Lines For Electric Railways, 3rd Edit., 116, John Wiley & Sons, 2018.
[51] S. Gregori, M. Tur, J.E. Tarancón, F.J. Fuenmayor, Stochastic Monte Carlo simulations of the pantograph–catenary dynamic interaction to allow for uncertainties introduced during catenary installation, Vehicle Syst. Dyn. 57 (4) (2019) 471–492, https://doi.org/10.1080/00423114.2018.1473617.
[52] Y. Song, P. Antunes, J. Pombo, Z. Liu, A methodology to study high-speed pantograph-catenary interaction with realistic contact wire irregularities, Mech. Mach. Theory 152 (2020), 103940, https://doi.org/10.1016/j.mechmachtheory.2020.103940.
[53] A. Gut. Probability: a graduate course, Springer, New York, 2005, https://doi.org/10.1007/B138932.
[54] Y. Song, F. Duan, Z. Liu, Analysis of critical speed for high-speed railway pantograph-catenary system, IEEE Trans. Veh. Technol. 71 (4) (2022) 3547–3555, https://doi.org/10.1109/TVT.2021.3136920.
[55] Y. Song, Z. Liu, H. Wang, X. Lu, J. Zhang, Nonlinear modelling of high-speed catenary based on analytical expressions of cable and truss elements, Veh. Syst. Dyn. 53 (10) (2015) 1455–1479, https://doi.org/10.1080/00423114.2015.1051548.
[56] A. Adhikari, A. Ram, R. Tang, J. Lin, Rethinking complex neural network architectures for document classification, in: NAACL HLT 2019 - 2019 Conference of the North American Chapter of the Association for Computational Linguistics: Human Language Technologies - Proceedings of the Conference 1, 2019, pp. 4046–4051, https://doi.org/10.18653/V1/N19-1408.
[57] M. Hardt, B. Recht, Y. Singer, Train faster, generalize better: stability of stochastic gradient descent, in: Proceedings of the 33rd International Conference on Machine Learning, ICML 2016, 2016.